



A knowledge augmented image deblurring method with deep learning for in-situ quality detection of yarn production

Chuqiao Xu ^a, Junliang Wang ^{b*}, Jing Tao ^c, Jie Zhang ^b and Ray Y. Zhong ^d

^aSchool of Mechanical Engineering, Shanghai Jiao Tong University, Shanghai, People's Republic of China; ^bInstitute of Artificial Intelligence, Donghua University, Shanghai, People's Republic of China; ^cCollege of Mechanical Engineering, Donghua University, Shanghai, People's Republic of China; ^dDepartment of Industrial and Manufacturing System Engineering, University of Hong Kong, Hong Kong, People's Republic of China

ABSTRACT

In the in-situ quality detection of yarn production, image deblurring plays a critical role in the vision-based detection systems to restore a sharp image and provide more accurate input for inspection. However, image deblurring is still challenging since the current methods are mainly based on the pre-defined blur degree. In dynamic yarn production, the relationship between the defocus blur degrees and the poses of the yarn body is highly associated, which can be excavated to prior knowledge in image deblurring to achieve more effective restoration. Thus, a knowledge augmented deep learning model is proposed to adaptively deblur yarn images with variable defocus blur degrees. A pose classification module designed by prior knowledge is embedded into the deep neural network, which classifies the yarn poses and feeds them into multi-scale deblurring channels. In each channel, we incorporate the image gradient prior into the specially designed loss function to attract the attention of the deblurring network on the edge details of the yarn. The experimental results from actual spinning processes demonstrate that the proposed method performs a better effect not only in the variable-scale deblurring of the global image but also in the restoration of the edge details.

ARTICLE HISTORY

Received 18 April 2021

Accepted 10 November 2021

KEYWORDS

Knowledge augmented; deep learning; image deblurring; machine vision detection; yarn production



1. Introduction

Product quality detection is an indispensable subject of production research (Genta, Galetto, and Franceschini 2020). In yarn production, product quality is unstable. Timely yarn quality detection is particularly important (Jing et al. 2020). With the development of machine vision and machine learning technologies (Perng, Lee, and Chou 2010; Rai et al. 2021), some pioneering works have been conducted to detect yarn quality replacing the traditional subjective human method (Guha et al. 2010; Li et al. 2017; Chen, Zhang, and Wu 2020). However, most of such studies capture and analyse yarn images in a stable experimental environment, resulting in inefficiency and lagged efforts when considering in-situ quality detection systems (Khan et al. 2019; Wang, Lee, and Angelica 2020). The current vision-based detection system is not capable of in-situ yarn detection because of the blurry images caused by high-speed rotation of the yarn. During yarn production, the spindle rotates at a high speed to twist the fibres into finer yarns with a certain geometric shape and mechanical properties, which drives the yarn space to revolve and jump. Thus, the

yarn will not be in the focal plane during the imaging process, which will produce out-of-focus blurry images for a vision-based detection system. Therefore, image deblurring (Wang et al. 2011) is a critical issue for in-situ quality detection in yarn production.

In general, the degradation process of the out-of-focus blurry image can be formulated by a standard model that the blurry image is equal to the convolution of the clear image and the blur kernel plus noise (Cheng et al. 2020). Recently, with the development of deep learning technology, some pioneering studies perform image deblurring by end-to-end networks (Cai, Zuo, and Zhang 2020; Wan et al. 2020; Wu et al. 2020; Zhao et al. 2020). These methods establish a fixed mapping between blurry and clear images from plenty of training data, which are attempt to build a general model that cover all out-of-focus blurred scenes.

In vision-based in-situ quality detection of yarn production, image deblurring remains a challenging task due to the following two aspects. **First**, the defocus distance of the yarn from the imaging focal plane is variable. As shown in Figure 1, in the yarn production process, the

CONTACT Jie Zhang  mezhangjie@dhu.edu.cn  Room 2-2406, No. 2999 Renmin North Road, Songjiang, Shanghai, China

*Present address: National Synthetic Fiber Engineering Technology Research Center, Beijing Chonglee Machinery Engineering Co., Ltd, Beijing, People's Republic of China

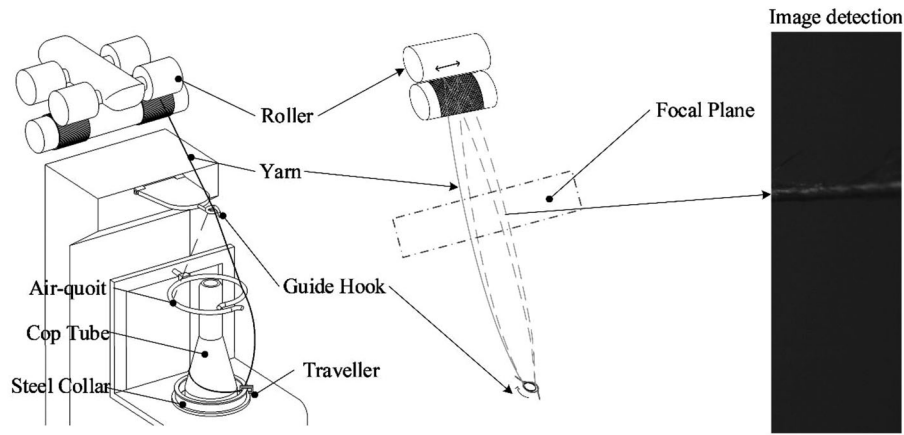


Figure 1. Vision-based in-situ quality detection during spinning.

roving is drafted into a finer yarn of about 0.2 mm by two sets of rollers with velocity differences. Meanwhile, the yarn is driven to rotate in space by the spindle. In this process, the yarn segment leaves the imaging focal plane at a cyclically changing distance, which causes blurred images in variable scales. Hence, how to deal with the *variable scale blur between images* is challenge. **Second**, in yarn quality detection, the edge detail information of the yarn body is crucial. The clarity of the yarn boundary directly affects the measurement accuracy of the quality indicators. However, the proportion of the yarn is small compared to the rest of background in the image. Hence, how to make the deblurring model *focus on the restoration of the edge details of the yarn body* instead of the background is another challenge.

This paper proposes a knowledge augmented deep learning model (KD-DeblurNet) for image deblurring to address the above two challenges. Firstly, the relationship between yarn poses and defocus blur degrees is investigated. This prior knowledge is taken to guide the construction of the deep neural network with multi-scale deblurring channels. Secondly, in each channel, we incorporate the image gradient prior into the specially designed loss function to attract the attention of the deblurring network on the edge details of the yarn. The main contributions of this work are summarised as follows.

- The corresponding relationship between the defocus blur degree and the pose of the yarn body in the vision-based detection systems is revealed, which provides a new view for improving the vision-based in-situ quality detection system.
- A knowledge augmented deep learning model is proposed for image deblurring in vision-based in-situ quality detection of yarn production, which provides a possible way for integrating the production knowledge into deep learning models in production research.

The rest of this paper is organised as follows. Section 2 reviews the significantly related works about image deblurring. Next, the proposed knowledge augmented deep learning model for image deblurring in vision-based in-situ quality detection of yarn production is detailed in section 3. Experimental results and discussions are demonstrated in section 4. Finally, conclusions and future work are summarised in section 5.

2. Related works

2.1. Prior knowledge-driven methods

The typical prior knowledge-driven methods of image deblurring mainly include Wiener filter algorithm (Luo et al. 2019) and Lucy-Richardson (LR) iterative deconvolution algorithm (Abang, Ramli, and Halim 2018). Wiener filter deblurring approach is based on the principle that the Fourier transform of the convolution of two functions equals the Fourier transform of the two functions. If the Fourier transform of the degradation model and the blurry image is known, the Fourier transform of the clear image can be obtained. Thus, the clear image can be restored through the inverse Fourier transformation.

Since the limitations of the above methods that the high-frequency information of sharp edges is lost, the maximum a posterior (MAP) methodology (Sha, Schonfeld, and Wang 2020; Zhou et al. 2020; Wang, Zhu, and Bai 2021) is developed with different likelihood functions and image priors. Over the years, numerous studies were devoted to carefully designing regularisation priors by domain knowledge. Beck and Teboulle (2009) derived a gradient-based shrinkage/thresholding algorithm based on the discretized total variation (TV) minimisation model with constraints for image deblurring. Yan et al. (2017) observed the phenomenon that the bright pixels in the clear images are not likely to be bright after

the deblurring process. Xu, Chen, and Li (2020) proposed an iteration-wise ℓ_p -norm regularisation strategy to enhance the salient edge selection of MAP image deblurring framework. Based on this observation, a joint prior (bright and dark channel prior) was proposed to obtain a sharp latent image during image deblurring. Zhang et al. (2021) used ℓ_0 -regularised gradient prior to improve the restoration ability of the sharp edge in natural image deblurring.

These knowledge-based regularisation priors are indeed beneficial to restore sharp edges of images. However, this kind of method requires complex derivation and iterative optimisation for each image with a different blur kernel, resulting in high computational costs and inefficient performance.

2.2. Data-driven methods

In recent years, with the success of deep learning (Kusiak 2020; Fan et al. 2021), some studies started to adopt data-driven methods to estimate the complicated blur kernel for image deblurring. Sun et al. (2015) adopted a convolutional neural network (CNN) composed of 6 layers of convolutional layers and fully connected layers to output the probability of each candidate motion kernel, which can effectively estimate non-uniform motion blur. Chakrabarti (2016) proposed a multi-resolution decomposition full connected neural network to predict the Fourier coefficients of a deconvolution filter, which encode the input patch into four 'bands' to successfully handle large blur kernels.

Some recent studies adopted data-driven methods for image deblurring by directly learning the end-to-end mapping relationship between blurry images and clear images from plenty of training data. Nah, Kim, and Lee (2017) proposed a deep multi-scale CNN embedded in multiple ResBlocks in each scale that took a blurry image pyramid as the input and output an estimated latent image pyramid, which outperformed in dynamic scene deblurring. Kupyn et al. (2018) developed a deblur generative adversarial network (DeblurGAN) based on the VGG19 network for blind motion deblurring, which was special in that it adopted a combined loss function to focus on restoring general content and texture details. However, to pursue better deblurring performance, the network structures became deeper and more complex. Thus, some latest studies suggested streamlining the network structures of image deblurring. Tao et al. (2018) proposed a scale-recurrent network (SRN) composed of a series of convolutional layers, ResBlocks, deconvolutional layers, and long short-term memory (LSTM). The advantage of SRN was that it had fewer parameters than previous multi-scale deblurring ones. Gao et al. (2019)

developed a selective sharing scheme for constraining the deblurring network structure (PSNC), which included 3 encoder stages and 3 decoder stages. It is composed of 3 kinds of modules including feature extraction, non-linear transformation, and feature reconstruction with a skip connection to achieve higher performance and fewer parameters for dynamic scene deblurring.

In summary, the data-driven deep neural networks for image deblurring, which mainly includes 3 modules of feature extraction (encoder), non-linear mapping, and reconstruction (decoder), are successful in image deblurring. However, this kind of method attempts to establish a general model that covers all blurred scenes while ignoring the details of sharp structures in images. Inspired by the literature, integrating knowledge-driven priors into deep learning models will be a possible solution for image deblurring in vision-based in-situ quality detection of yarn production.

3. Proposed method

This section introduces the proposed knowledge augmented deep learning model for image deblurring in in-situ yarn quality detection, which includes three parts. We firstly investigate the movement of yarn in spinning to analyse the defocusing phenomenon. Next, a deep neural network with multi-scale deblurring channels is constructed under the guidance of the yarn defocus distribution. Finally, the details of deblurring model implementation are introduced.

3.1. Defocus analysis of the yarn movement in the spinning process

Binocular cameras are used to capture high-frequency yarn images during spinning to obtain the spatial coordinates of the yarn movement points. Fit the movement trajectory and analyse the corresponding yarn image sharpness distribution of the yarn movement. It is implemented in 5 steps, as shown in Figure 2.

• Step 1: Deploy binocular cameras.

Two cameras of the same type are used to capture images of the yarn simultaneously from the front and side of the spinning spindle.

- (1) Place the two cameras at a 90-degree angle.
- (2) Keep the same parameter settings for the two cameras.
- (3) Use a calibration plate to ensure that the two cameras are at the same height and shooting in the same area.

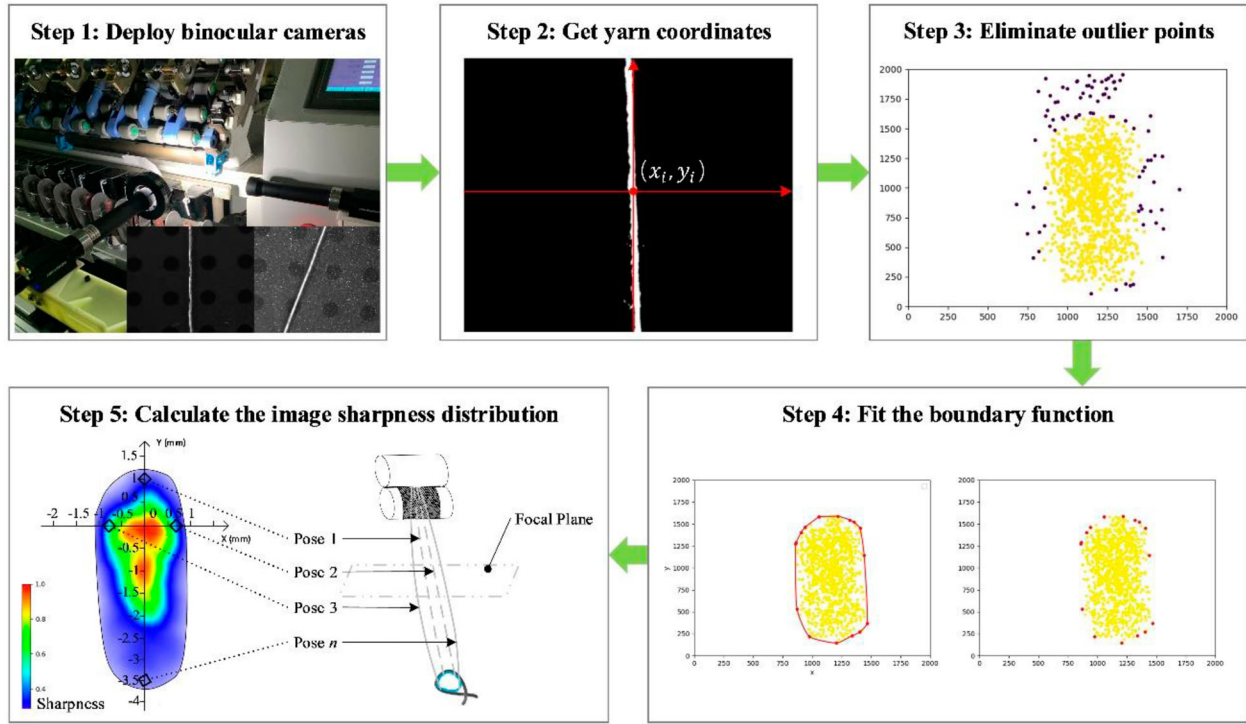


Figure 2. Defocus analysis of the yarn movement in the spinning process.

- (4) Use the hardware trigger signal to control the two cameras to shoot at the same time.

• **Step 2: Get yarn coordinates.**

For the two images obtained at each shooting moment, taking the yarn centre of the image captured by the front camera as the x coordinate and the yarn centre of the image captured by the side camera as the y coordinate, the spatial coordinates of the yarn position at this moment can be obtained. The collection of the coordinates of all captured images forms a point cloud covering the movement of the yarn.

- (1) Use OSTU (proposed by Nobuyuki Otsu) threshold segmentation algorithm (Zhong and Ma 2021) to binarize the captured greyscale images. Assuming that the segmentation threshold of yarn and background is t , the proportion of yarn pixels in the image is w_0 , and the mean is u_0 . The proportion of background pixels in the image is w_1 , and the mean is u_1 . Then, the mean value of the whole image is going to be:

$$u = w_0 * u_0 + w_1 * u_1. \quad (1)$$

The objective function is defined as:

$$g(t) = w_0 * (u_0 - u)^2 + w_1 * (u_1 - u)^2. \quad (2)$$

Where $g(t)$ is the expression of the variance between classes when the segmentation threshold is t . When $g(t)$

get the maximum, the corresponding t is the optimal threshold.

- (2) Perform opening and closing operations on the binary image to obtain a connected area.
- (3) Calculate the border of the connected area, the border of the connected area with the largest area is the border of the yarn backbone. Average the coordinates of the left and right limit positions of the yarn backbone border is the yarn centre coordinates.
- (4) Combine the x coordinate of the front image and the y coordinate of the side image to get the space point coordinates of the yarn at that moment. The collection of spatial point coordinates on the time series forms a spatial point cloud covering the movement of the yarn.

• **Step 3: Eliminate outlier points.**

- (1) Use LOF (local outlier factor) algorithm to detect outliers in the yarn movement point cloud and eliminate them.
- (2) Calculate the local outlier factor for each point p in the point cloud.

$$LOF_k(p) = \frac{\sum_{o \in N_k(p)} \frac{lr_d_k(o)}{lr_d_k(p)}}{|N_k(p)|} \quad (3)$$

Where $LOF_k(p)$ represents the average ratio of the local reachable density of the neighbouring point $N_k(p)$ to the

local reachable density of the point p . The local reachable density of the point p can be expressed by the following formula. The local reachable density $lrd_k(p)$ can be calculated by the following formula.

$$lrd_k(p) = 1 / \left(\frac{\sum_{o \in N_k(p)} reach_dist_k(p, o)}{|N_k(p)|} \right) \quad (4)$$

Where $reach_dist_k(p, o)$ denotes the k th reachable distance from point o to point p , which can be calculated by the following formula.

$$reach_dist_k(p, o) = \max\{k_dist(o), d(p, o)\} \quad (5)$$

Where $k_dist(o)$ represents the k th distance, that is, the distance of the k th point away from p , excluding p . $d(p, o)$ represents the two points p and o .

- (3) If $LOF_k(p) \neq 1$, then, point p is regarded as an outlier and eliminated from the yarn movement point cloud.

- **Step 4:** Fit the boundary function.

- (1) Use the Graham scan algorithm (Ferrada, Navarro, and Hitschfeld 2020) to find the discrete points that form the smallest convex hull of yarn movement point cloud.
- (2) Use the B-spline curve (Xu et al. 2020) to piecewise fit a smooth boundary of selected discrete points with the smallest convex hull.
- (3) Use the least squares method to fit the movement trajectory of the yarn through the points on the time series, which is a longitudinal reciprocal movement of approximately elliptical.

- **Step 5:** Calculate the image sharpness distribution.

- (1) Use the variance function to evaluate the sharpness of the segmented yarn trunk image.

$$D(f) = \sum_y \sum_x |f(x, y) - \overline{f(x, y)}|^2 \quad (6)$$

Where $D(f)$ is the calculation result of the image sharpness, $f(x, y)$ is the grey value of the pixel (x, y) corresponding to the image f , and $\overline{f(x, y)}$ represents the average grey value of the entire image.

- (2) To avoid the function value being affected by the image size, the results of the image sharpness $D(f)$ are divided by the number of pixels to be normalised.

$$\widetilde{D(f)}_i = \frac{1}{n} * \frac{D(f)_i - D(f)_{min}}{D(f)_{max} - D(f)_{min}} \quad (7)$$

Where $\widetilde{D(f)}_i$ denotes the normalised sharpness of image i , n is the number of pixels in the image i , $D(f)_i$ is the original sharpness of image i before normalised, $D(f)_{max}$ and $D(f)_{min}$ respectively represent the maximum and minimum original sharpness in all images.

- (3) According to the sharpness of all captured points, calculate the sharpness distribution of images in the yarn movement. Establish the correspondence between the pixel coordinate system and the world coordinate system. Map the sharpness value of each point to the corresponding colour value to draw a heat map in the world coordinate system, which reflects the mapping relationship between the yarn movement position and the defocus blur degree of the imaging system in the actual spinning process.

Based on the above analysis, it is found that the yarn movement in the ring spinning process is an elliptical trajectory of reciprocating translation, which causes the image out-of-focus blur degree to spread to the surroundings with the guide hook as the centre. Since the yarns at different positions have different coordinate ranges and inclination angles (called pose in this paper), that is, the poses of the yarns are closely related to the degree of out-of-focus blur. As shown in Table 1, the movement poses are divided into 11 categories according to the quadrants, directions, and inclination angles of the yarn. Then, the categories are mapped to 4 degrees of blur, according to the corresponding imaging sharpness distribution heat map. Since various degrees of blur correspond to differential deblurring functions (non-linear mapping relationship between blurred images and clear images), this prior knowledge can be used to guide the construction of the yarn image deblurring network. The pose of the yarn can be recognised from the captured image to determine the defocus blur degree of the image. Then, images with different defocus degrees can be fed into different deblurring channels to separately establish the mapping relationship between blurred images and clear images.

3.2. Deblurring network integrating prior knowledge of yarn movement

Based on previous deep neural networks for image deblurring, the main functional structures of encoder modules, non-linear mappings, and decoder modules are worked out. Specifically, a pose classification module is designed to distinguish the different movement poses, which have different degrees of defocus blur. Additionally, a pose gate is designed to send the extracted features to the corresponding reconstruction channel according to the pose category, where different reconstruction

Table 1. The relationship between yarn poses and defocus degrees.

Quadrant	Direction	Inclination angles	Blur degree
I	Front	$0^\circ \sim 7^\circ$	Low & Middle (2)
I	Front	$> 7^\circ$	High (4)
II	Backward	$0^\circ \sim 7^\circ$	Low (1)
II	Backward	$7^\circ \sim 20^\circ$	Low & Middle (2)
II	Backward	$> 20^\circ$	High (4)
III	Backward	$0^\circ \sim 7^\circ$	Low (1)
III	Backward	$7^\circ \sim 20^\circ$	Low & Middle (2)
III	Backward	$> 20^\circ$	High (4)
IV	Front	$0^\circ \sim 7^\circ$	Low & Middle (2)
IV	Front	$7^\circ \sim 20^\circ$	Middle & High (3)
IV	Front	$> 20^\circ$	High (4)

channels learn different deblurring mappings. A reconstruction gate is also designed to integrate the reconstruction information from all channels to generate a clear image. Furthermore, the loss function of the network is improved by adding a ℓ_0 -regularised gradient prior to strengthen the restoration ability of the sharp edge of the yarn.

3.2.1. Network structure

The proposed KD-DeblurNet, as shown in Figure 3, consists of an input layer, 3 modules (feature extraction module, pose classification module, and reconstruction module), 2 gates (pose gate and reconstruction gate), and an output layer. The inputs of the network are blurry images, and the outputs are corresponding clear images. The feature extraction module is composed of 3 convolutional layers (CONV.) and 1 max pooling layer (MAXP.). The Pose classification module is composed of 2 fully connected layers (FC.), where the last fully connected layer outputs the categories of yarn poses. Pose gate outputs the blur features of the yarn pose to the corresponding reconstruction channel. The reconstruction

module is composed of multiple channels, and each channel that represents different out-of-focus blur mapping includes 3 consecutive deconvolution layers (DECONV.). The reconstruction gate integrates the information from all channels to output a clear image. The detailed network structure parameters are shown in Table 2, some of which refer to (Tao et al. 2018).

Input layer: the input $X_{h \times w \times c}$ of the network is the blurry image, which is a pixel matrix. h and w are the height and width of the image, c is the number of image channels.

Feature extraction module: the feature extraction module is an alternately transmitting operation through 3 convolutions, batch normalizations, and nonlinear activation functions. The convolutional layer extracts blur features from the input blurry image by convolutional kernels to transform the input image into multivariate feature maps.

$$H_{ij} = \sum_{m=1}^r \sum_{n=1}^r K_{mn} X_{(m+i \times l)(n+j \times l)} + B, \quad (8)$$

$$0 \leq i \leq \frac{h-k}{l}, 0 \leq j \leq \frac{w-k}{l}.$$

Where H denotes the extracted feature map through the convolution operation, i, j are the position coordinates of the feature map matrix. K represents the convolution kernel of size $r \times r$. X is the pixel matrix of the input blurry image. l denotes the stride length of the convolution kernel's movement. B is the bias. h and w are the height and width of the input image respectively. Then, H is batch normalised and activated by *BatchNorm* and *Relu* functions.

The third convolutional layer is followed by a max pooling layer, which is used to undersample the features extracted by the convolutional layer to reduce the size of

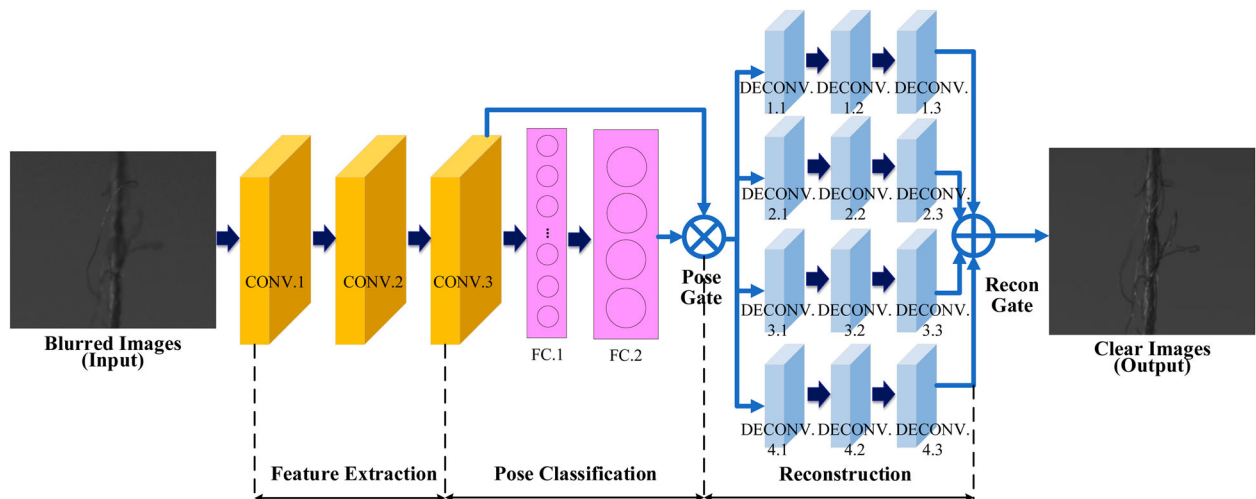
**Figure 3.** The network structure of proposed KD-DeblurNet.

Table 2. The network structure parameters of the proposed KD-DeblurNet.

Layer	Size	Filters	Stride	Input	Output
CONV.1	5*5	32	1	796*2448*3	796*2448*32
CONV.2	5*5	64	2	796*2448*32	398*1224*64
CONV.3	5*5	128	1	398*1224*64	398*1224*128
MAXP.	2*2	/	2	398*1224*128	199*612*128
FC.1	/	1024	/	199*612*128	1024
FC.2	/	4	/	1024	4
DECONV.1	3*3	64	2	199*612*128	398*1224*64
DECONV.2	3*3	32	2	398*1224*64	796*2448*32
DECONV.3	5*5	3	1	796*2448*32	796*2448*3

Table 3. The key technical parameters of the camera and telecentric lens.

Camera parameters	Value	Telecentric lens parameters	Values
Type of sensor	2/3" CMOS	Magnification	1.0
Resolution rate	2448*2048	Focal length	110 mm
Pixel size	3.45 μm \times 3.45 μm	Format	$\Phi 11$ mm (2/3)"
Frame rate	23.5 fps	Field angle	D: 11 mm H: 8.8 mm V: 6.6 mm
Data interface	Gigabit Ethernet	Mount	C

the feature map and suppress the overfitting. After the above three sets of convolution and pooling operations, $n * n$ feature maps extracted from the blurry image are available. The feature maps are fed into the pose classification module and the pose gate respectively, which hit two birds with one stone.

Pose classification module: the pose classification module is used to classify the types of yarn movement poses from the extracted feature maps of blurry images. As shown in Table 1, there are 11 types of movement poses. Since one or more poses correspond to a fixed blur degree, these types are divided into 4 blur degrees. Therefore, the blur degrees of the yarn can be classified according to its poses, which is beneficial for customising exclusive reconstruction channels for images with different blur degrees. During the model training, images will be labelled with categories of blur degrees to guide the pose classification module to learn the discrimination ability of pose and blur degree.

The pose classification module is composed of 2 fully connected layers. In this module, the extracted feature maps of a blurry image are unified into one dimension. Then, the unified features are performed nonlinear mapping by the first fully connected layer and output the probability of belonging to each pose category by the second full connected layer.

$$H^{(k)} = \delta(w^{(k)}H^{(k-1)} + b^{(k)}) \quad (9)$$

Where $H^{(k)}$ represents the hidden representation of k th full connected layer. δ denotes the nonlinear activation function *Relu*. $w^{(k)}$ and $b^{(k)}$ are the weights and bias of the

k th full connected layer, respectively. The first connected layer is composed of 512 neurons. The second connected layer is composed of C neurons, which are equal to the categories of blur degrees.

Pose gate: the pose gate sends the extracted feature maps to the corresponding reconstruction channel according to the pose category of the yarn in the image, which is achieved by multiplying the feature map and the probabilities that the feature map belongs to the corresponding pose category.

$$P_i = H_i^{(k)} \cdot H, i \in [1, 2, \dots, C] \quad (10)$$

Where P_i represents the probabilistic feature map. It is the product of the feature map H and the probability $H_i^{(k)}$ while the feature map belongs to the i th category. P_i is close to 0 when H does not belong to the i th category. On the contrary, when H belongs to the i th category, P_i is close to 1. Thus, we can obtain C probabilistic feature maps through pose gate.

Reconstruction module: the reconstruction module is composed of C reconstruction channels. The i th probabilistic feature map is fed into i th reconstruction channels. Each reconstruction channel is composed of 3 deconvolutional layers to reconstruct the clear features by deconvolving the feature maps.

$$S_i = D_i^T P_i, i \in [1, 2, \dots, C] \quad (11)$$

Where S_i denotes the reconstructed clear features at i th channel. D_i^T denotes the deconvolution operation, which is the reverse of convolution $P_i = D_i S_i$.

Reconstruction gate: the reconstruction gate assembles the clear features of each reconstruction channel to output the sum of all clear features.

$$Y = \sum_{i=1}^C S_i \quad (12)$$

Output layer: the output $Y_{h \times w \times c}$ of the network is the clear image of the same size as the original blurry image.

3.2.2. Loss function

In the backward propagation process during training, the network parameters are optimised according to the gradient of the loss function and the learning rate to minimise the loss.

$$\theta^{(k+1)} = \theta^{(k)} - \alpha \frac{\partial \text{loss}}{\partial \theta^{(k)}} \quad (13)$$

Where $\theta^{(k)}$ denotes the values of network parameters in k th iteration. α is the learning rate, which is used to control the amplitude of each optimisation and find the optimal solution. *loss* is the loss function network, which

is the optimal object of the deblurring model. In general, the loss function is the mean squared error between networks' output values and ground truth.

$$\text{loss}_o = \frac{1}{N} \sum_{i=1}^N (y_i - \hat{y}_i)^2 \quad (14)$$

Where y_i denotes the original clear images. \hat{y}_i represents the output deblurred images of the proposed model. N is the batch size, which means the number of training samples fed in each iteration. loss_o aims to minimise the overall error between the blurry images and the original clear images.

Since the detailed edge restoration of the yarn body is focused instead of the background, we improved the general loss function by adding a loss of ℓ_0 -regularised gradient prior to attract the attention of the deblurring network on the edge details of the yarn.

$$\text{loss} = \text{loss}_o + \lambda \cdot \text{loss}_{\ell_0} \quad (15)$$

Where λ is a weight coefficient to balance two losses. loss_{ℓ_0} is a difference of regularisation term of pixel gradients between original clear images and output deblurred images.

$$\text{loss}_{\ell_0} = \frac{1}{N} \sum_{i=1}^N (\|\nabla y_i\|_0 - \|\nabla \hat{y}_i\|_0)^2 \quad (16)$$

Where $\|\nabla y_i\|_0$ counts the number of nonzero-intensity pixels in y_i . With this intensity property, the sharp edge and background of images can be differentiated. The pixel gradient value of the background area of the image is mostly 0, while the pixel gradient of the sharp edge is non-zero. The pixel gradient of images is calculated by the Sobel operator.

$$\nabla y_{(u,v)} = \sqrt{G_u^2 + G_v^2} \quad (17)$$

Where G_u is the pixel gradient in the horizontal direction, and G_v is the pixel gradient in the vertical direction.

$$\begin{aligned} G_u &= \frac{\partial f}{\partial u} = [f(u+1, v-1) + 2 * f(u+1, v) \\ &\quad + f(u+1, v+1)] - [f(u-1, v-1) \\ &\quad + 2 * f(u-1, v) + f(u-1, v+1)] \quad (18) \\ G_v &= \frac{\partial f}{\partial v} = [f(u-1, v-1) + 2 * f(u, v-1) \\ &\quad + f(u+1, v-1)] - [f(u-1, v+1) \\ &\quad + 2 * f(u, v+1) + f(u+1, v+1)] \quad (19) \end{aligned}$$

Where $f(u, v)$ denotes the pixel value at (u, v) coordinates of the image.

3.3. Deblurring model implementation

The procedures of model implementation are illustrated in Figure 4, which is composed of 3 steps.

(1) Data collection

A yarn image collection platform is constructed as shown in Figure 5. The key technical parameters of the camera and telecentric lens are detailed in Table 3. Adjust the front and rear distance of the camera making the imaging focal plane of the camera fall on the middle of the yarn motion range. Based on the analysis of the yarn movement, we simulate the various positions of the yarn in the motion range. At each position, we first take an initial blurry image, and then a clear image by adjusting the camera's focus. Hence, pairs of 'blurry-clear' yarn image data could be obtained.

(2) Model training

Pytorch is used to establish the proposed network structure, which is trained by the collected data to learn the nonlinear relationships between the blurry and clear images. The Adam optimiser is employed to optimise the parameters of the network to minimise the loss function. The training parameter settings obtained by a sensitivity analysis are list in Table 4.

(3) Statistical evaluation

After training, the network should be tested by the test data to evaluate the deblurring performance. The quantitative measure of peak-signal-to-noise ratio (PSNR), which is the most common and widely used objective measurement method for evaluating image quality, is employed to evaluate the quality of recovered images. PSNR is defined as follows.

$$\text{PSNR} = 10 \cdot \log_{10} \left(\frac{\text{MAX}_I^2}{\text{MSE}} \right) \quad (20)$$

Where MAX_I represents the maximum value of the image pixel. In our images, MAX_I is equal to 255. MSE denotes the mean squared error between the original clear image and the processed image.

$$\text{MSE} = \frac{1}{h \times w \times c} \sum_{k=1}^c \sum_{j=1}^w \sum_{i=1}^h (X_{i,j,k} - Y_{i,j,k})^2 \quad (21)$$

Where h and w are the height and width of the image, c is the number of image channels. $X_{i,j,k}$ is the pixel value of the original clear image at (i, j, k) coordinate. $Y_{i,j,k}$ is the pixel value of the processed image at (i, j, k) coordinate.

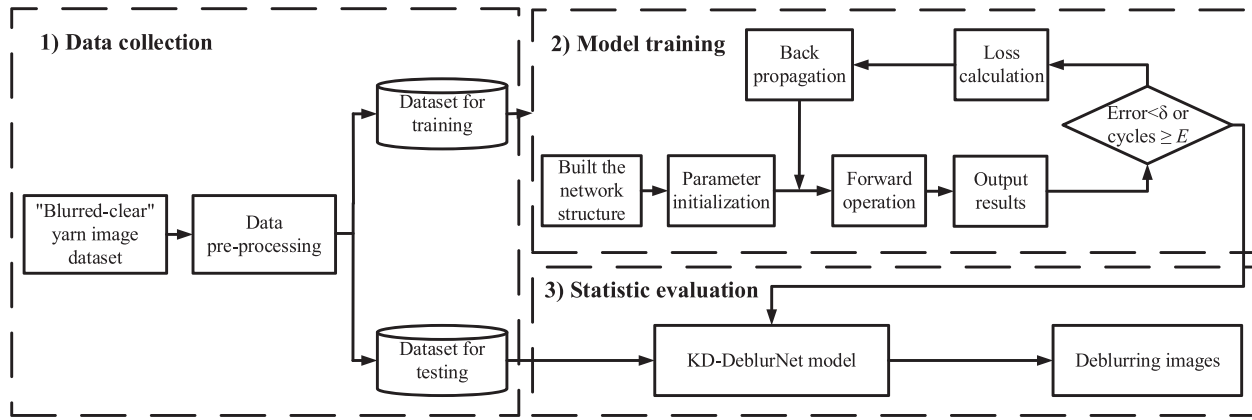


Figure 4. The procedures of the proposed model implementation.

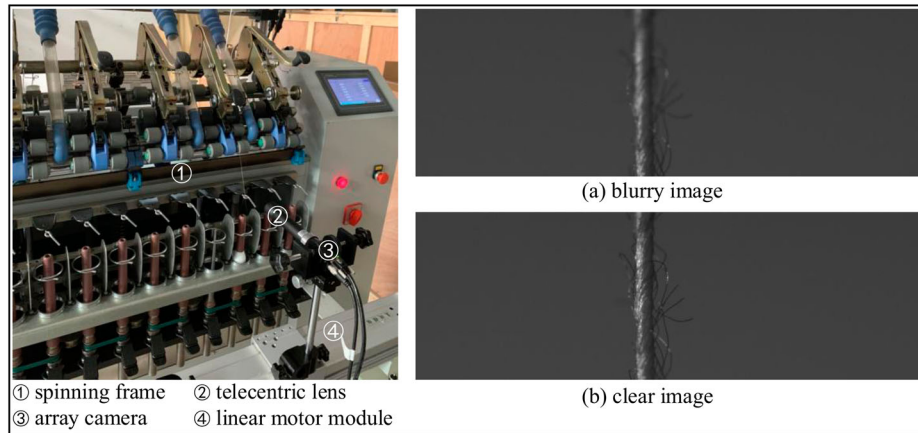


Figure 5. The yarn image collection platform.

Table 4. Parameter settings of the network training.

Hyperparameter	Symbol	Values
Maximal epochs	E	200
Batch size	b	16
Learning rate	α	0.001
The number of neurons in the last layer of the pose classifier	C	4
Weight coefficient of the loss function	λ	1/2448/100

Note that the higher the PSNR value, the less distorted the image will be. In general, PSNR below 20 dB is not acceptable for images. 20–30 dB indicates poor image quality. 30–40 dB usually indicates that the image quality is good (the distortion is detectable but acceptable). PSNR higher than 40 dB indicates that the image quality is very close to the original image.

4. Experimental results and discussion

To verify the effectiveness of the proposed method, experiments in the actual spinning process are conducted. The statistical information of the dataset is provided in Table 5. 80% of the collected images are taken

Table 5. The statistical information of the dataset.

Characteristics	Attributes/values	Unit
Dataset name	Yarn deblurred dataset	/
Data type	Greyscale image	/
Data format	Bitmap	.bmp
Number of instances	800	pair
Size	2448*796	pixel

as training data, 10% are used for validation and the remaining 10% are used for the performance testing. The deblurring network is conducted on a computer server with the following option: the Linux system is used with a Tesla V100 PCIe 32GB GPU card. The algorithm is compiled with Python 3.0, Pytorch1.8, and CUDA 10.2.

4.1. Deblurring performance comparison

To verify the efficiency of the proposed method for image deblurring, it is compared with the state-of-the-art prior knowledge-driven and deep learning deblurring methods, respectively.

(2) Comparison with prior knowledge-driven methods

In this section, the proposed method is compared with prior knowledge-driven deblurring methods such as Wiener filter (WF) (Luo et al. 2019), LR iterative deconvolution (LR) (Abang, Ramli, and Halim 2018), and ℓ_0 -regularised prior methods (ℓ_0 -R) (Zhang et al. 2021). We summarise the statistical performance and visual comparisons of each method for the test phase through 10-fold cross validation, which are respectively reported in Figure 6.

Figure 6(a) shows the statistics of the averaged peak-signal-to-noise ratio of images deblurred by comparison methods and the original blurry images (input) in the test set. The proposed method achieves the highest PSNR compared with the original blurry images and typical knowledge-driven deblurring methods. That indicates the effectiveness of the proposed method for deblurring the entire yarn image in such a dynamic spinning scene with variable-scale defocusing. On the contrary, the PSNR of WF and LR methods are worse than the original blurry images. It is indicated that the simple kernel estimation method is not suitable for this kind of variable-scale blurred scene, and even has a counterproductive effect of noise (as shown in Figure 6(c)). The ℓ_0 -R method has an average improvement of 0.6828 in PSNR compared with the original blurry images, which demonstrates the regularisation method with constraints has a slight deblurring effect in this variable-scale blurred scenario.

Figure 6(b) shows the pixel intensity distributions of gradient elements generated from the blurry image (input), clear image (ground truth), and deblurred images. The zero values of images gradients with sharp edges are denser than those of blurry ones. As it can be seen, the ℓ_0 -R method has the steepest peak around the 0 value, which indicates that the regularised intensity and gradient prior is beneficial to restore sharp edges of images. However, the gradient curve of ℓ_0 -R method is far away from the ground truth, which illustrates that the ℓ_0 -R method focuses more on the edges of an image but has some distortions in the variable-scale deblurring of the entire image (as shown in Figure 6(c)). In contrast, benefiting from the improved loss function, our proposed method can better fit the gradient curve of the ground truth, which is visualised in Figure 6(c).

(1) Comparison with deep learning methods

In this section, the proposed method is compared with deep learning methods such as CNN (Sun et al. 2015), DeblurGAN (Kupyn et al. 2018), SRN (Tao et al. 2018), and PSNC (Gao et al. 2019). The experimental results

of quantitative and visual comparisons for the test phase through 10-fold cross validation are respectively reported in Figure 7.

From Figure 7(a), SNR, PSNC, and the proposed method outperform CNN and DeblurGAN on PSNR, which proves the effectiveness of multi-scale deblurring network structures for deblurring the entire yarn image in such dynamic spinning scene with variable-scale defocusing. In particular, the proposed method achieves the highest PSNR, which is 0.3354 higher than the state-of-the-art PSNC method on average with images of 2448*2048 pixels. From Figure 7(b), the nonzero gradient values of comparison data-driven methods are denser than those of the ground truth. It shows that the current data-driven deblurring networks aim to minimise the average error of the overall pixel values while ignoring the ability to restore the edges of the image. Although the SNR and PSNC methods have good effects on deblurring the entire image, they are not enough to restore the edges of the image. In contrast, the proposed method has the steepest peak around the 0 value and fits the gradient curve of the ground truth well, which indicates that the proposed method keeps the global variable-scale deblurring ability while paying attention to the restoration of image edges. It can be seen from the visual comparisons in Figure 7(c).

4.2. Quality detection performance comparison

To verify the model for quality detection, the proposed method is compared with the state-of-the-art deblurring methods in the quality index of yarn evenness. Yarn evenness is one of the most important yarn quality indicators, which refers to the uniformity of the yarn body diameter along the axial segment. The yarn body diameter can be calculated by counting the pixels in each row of the image that belong to the yarn body. Then, the coefficient of variation (CV) of diameters is used to evaluate the quality of the yarn.

$$CV = \sqrt{\frac{1}{Q} \sum_{i=1}^Q (d_i - \bar{d})^2} \div \bar{d} \quad (22)$$

Where Q is the number of yarn body diameters taken within a fixed yarn length, and \bar{d} represents the average value of the yarn body diameters.

In the experiment, the CV value calculated from deblurred images is compared with the results detected by the laboratory precision instrument. The mean relative error (CV-MRE) is employed as the evaluation metrics. Comparisons of different deblurring methods are made in terms of such fashion. The quantitative results are reported in Table 6.

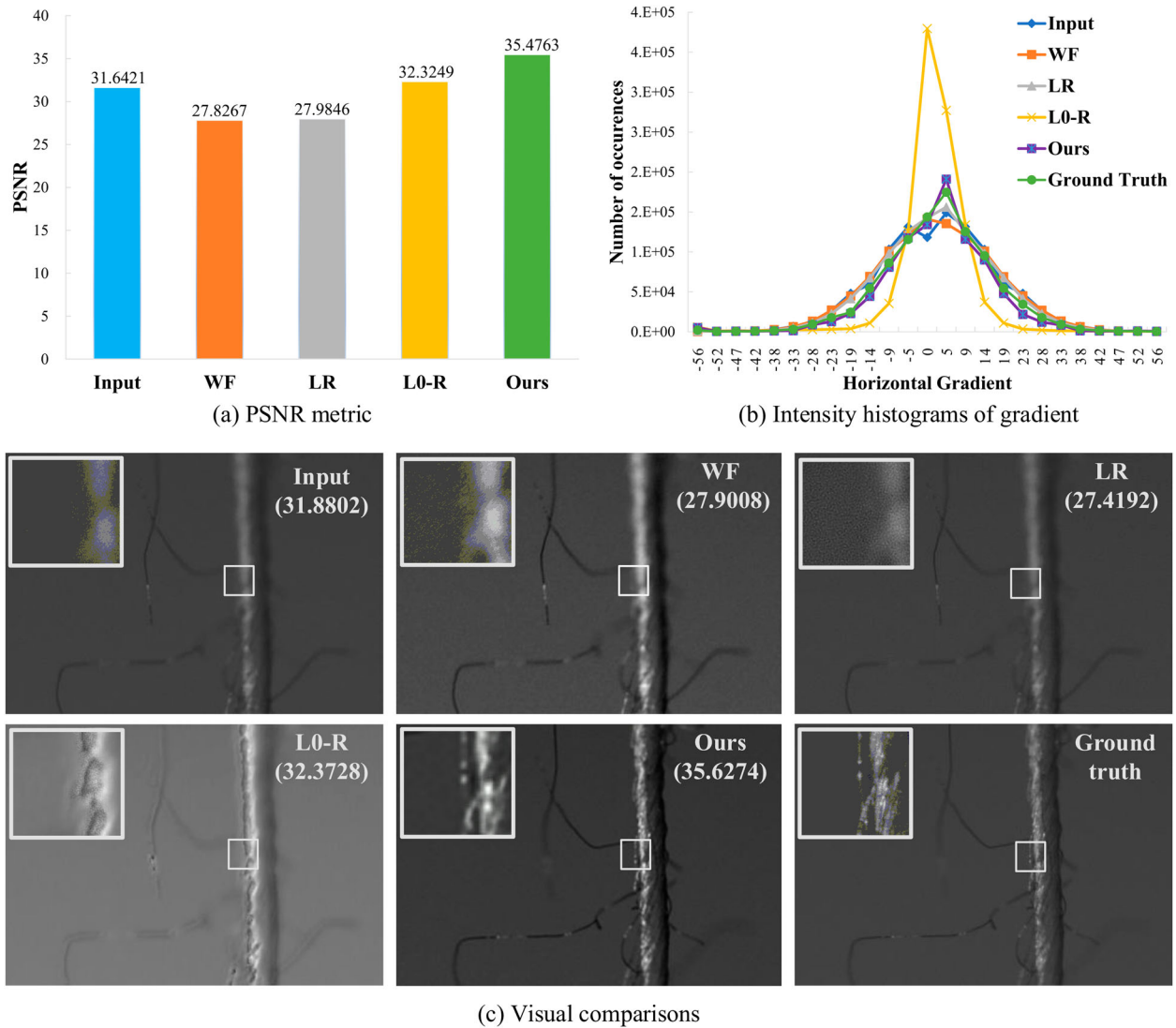


Figure 6. Comparisons of the proposed KD-DeblurNet and knowledge-driven methods.

It can be seen that the proposed method gets an error ratio of less than 1% on the quality index. Meanwhile, it is found that the error on the quality index is not completely positively correlated with the overall sharpness of the image (PSNR). This echoes that the edge detail information of the yarn body is more crucial in yarn quality detection. The proposed model focuses on the restoration of the edge details of the yarn body instead of the background, which outperforms other methods in quality detection.

4.3. Running time comparison

Considering the timely requirements of online quality detection, the running time is compared with the state-of-the-art deblurring methods on the same platform

(Tesla V100 PCIe 32GB GPU). For the deep-learning-based approach, the trained model is directly used in the actual detection process. Therefore, the training time is not included in the detection time except the time interval between the input of a blurred image and the output of a clear image. The quantitative results are reported in Table 6.

The results show that the detection time of the proposed method is 0.7534 seconds, which is not superior compared to other methods due to the multi-channel structure increasing the amount of parameter calculation. However, for the actual industrial application, the proposed method is feasible. The detection frequency is 1 second which will process 1 image within a second. Adding 0.0426 seconds for the camera to take an image, the total time of the proposed method for each detection

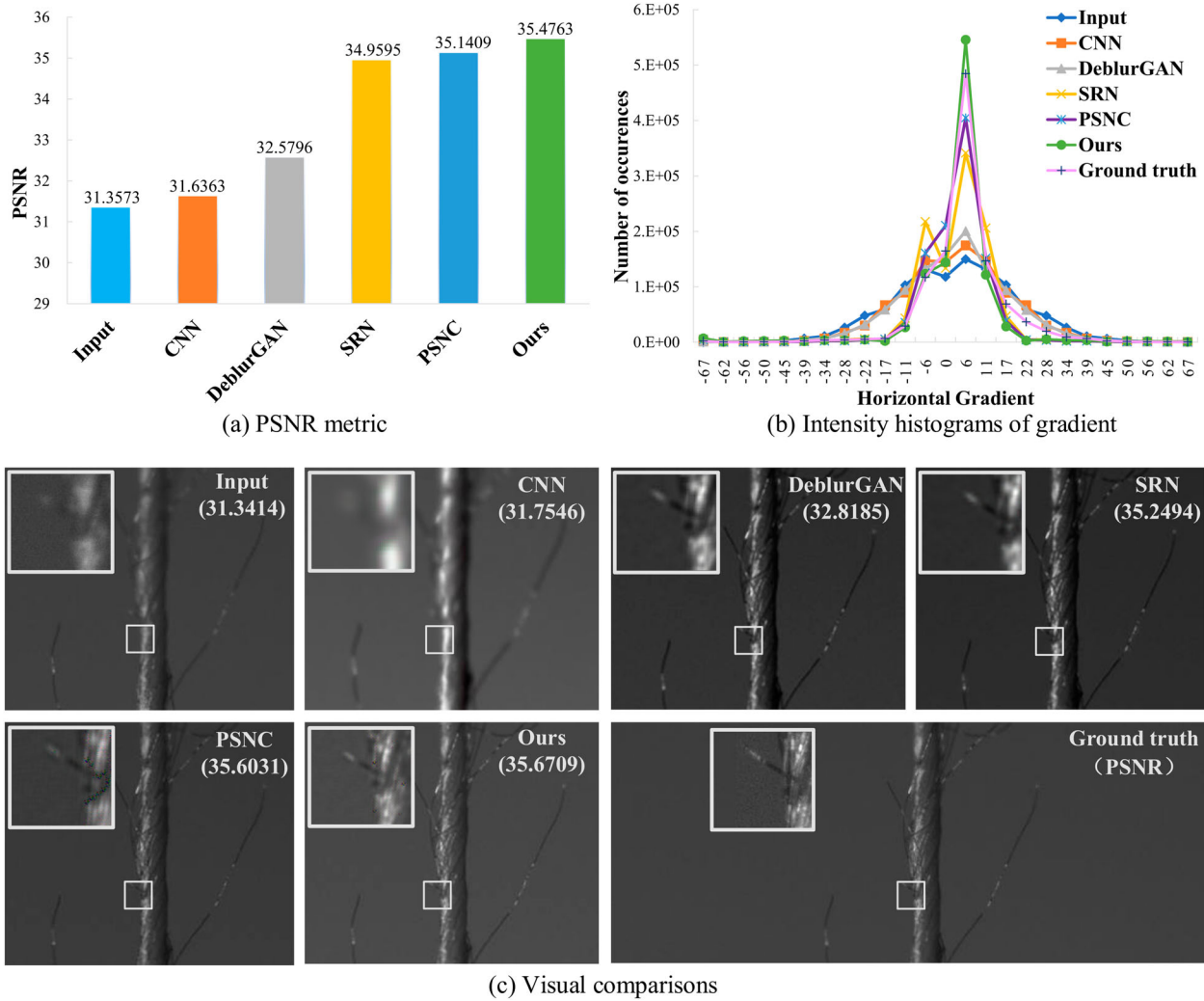


Figure 7. Comparisons of the proposed KD-DeblurNet and data-driven methods.

is less than 1 second, which can meet the requirements of online detection.

4.4. Discussion

(1) Parameter settings

The proposed model involves three main parameters, α (learning rate), C (the number of neurons in the last layer of the pose classifier), and λ (weight coefficient of the loss function). In this section, the parameter setting for model training will be discussed via sensitivity analysis.

For each parameter, experiments are conducted with different parameter settings by varying one and fixing others with the PSNR metric. For parameter α , the value is set from 10^{-5} to 10^{-1} with the increment of a multiple of 10. For parameter C , it is set from 1 to 10 with the step size of 1. For parameter λ , value is from $10^{-4} \times 1/2448$ to $1/2448$ with the increment of a multiple of 10, where

Table 6. Quantitative comparison of the proposed method with the state-of-the-art deblurring methods on comprehensive indicators.

Methods	PSNR	CV-MRE (%)	Detection time (s)
WF (Luo et al. 2019)	27.8267	6.2408	0.6211
LR (Abang, Ramli, and Halim 2018)	27.9846	5.6121	0.2450
ℓ_0 -R (Zhang et al. 2021)	32.3249	6.7977	0.2753
CNN (Sun et al. 2015)	31.6363	5.2860	0.1148
DeblurGAN (Kupyn et al. 2018)	32.5796	4.0478	1.9473
SRN (Tao et al. 2018)	34.9595	2.2564	0.6210
PSNC (Gao et al. 2019)	35.1409	1.3829	0.3960
KD-DeblurNet (Ours)	35.4763	0.9040	0.7534

2448 is the number of pixels in the image. Figure 8 shows the sensitivity analysis results of α , C , and λ . The parameter setting with higher PSNR and lower computational overhead is selected for model training. For the learning rate α , the lower the value, the greater the computational cost due to the shorter convergence step. When it is lower than 10^{-3} , the PSNR is basically the same, so we choose 10^{-3} as its parameter setting. For the number of pose

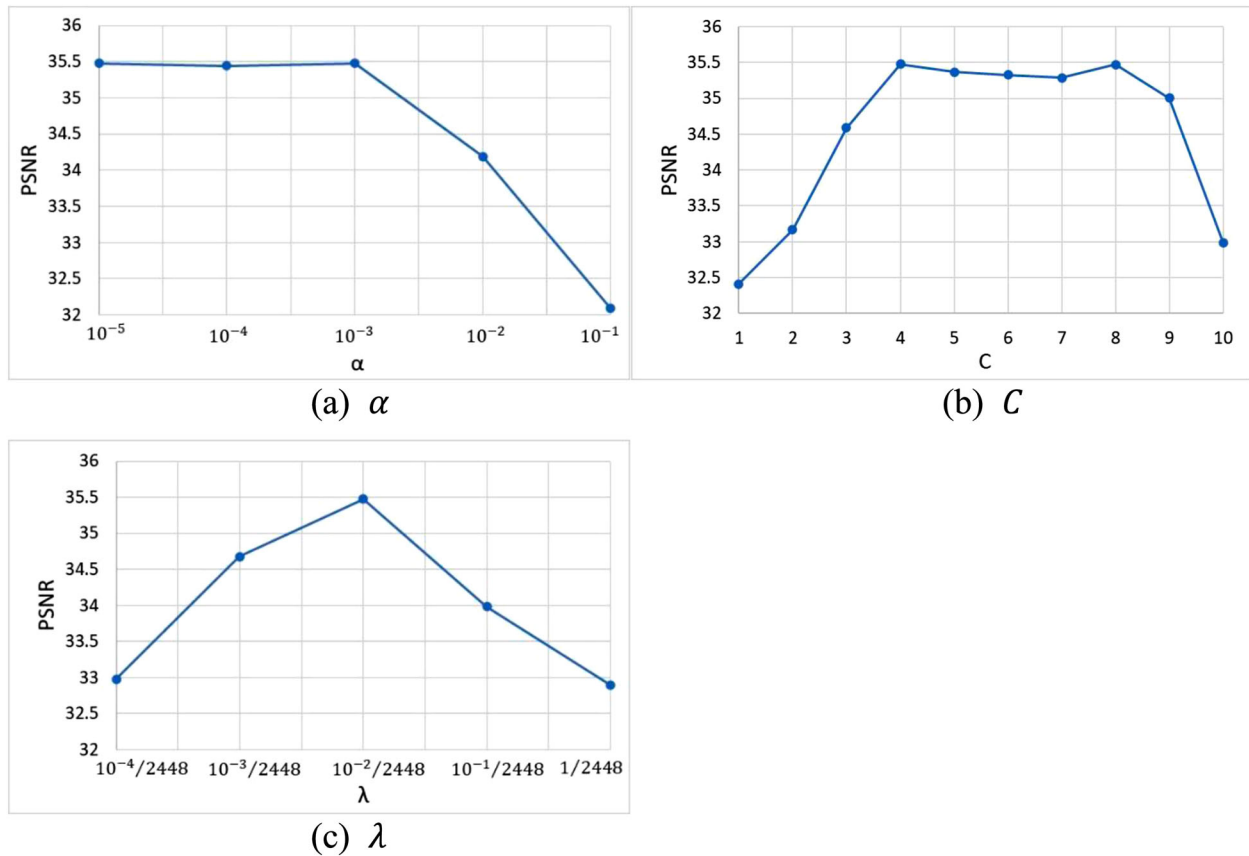


Figure 8. Sensitivity analysis of α , C , and λ for the proposed model.

categories C , the higher the value, the greater the computational cost due to more reconstruction channels. When it is between 4 and 8, higher PSNR will be achieved, so we choose 4 as its parameter setting. For the weight of coefficient of loss function λ , its value does not affect the calculation overhead, so we choose $10^{-2} \times 1/2448$ as its parameter setting due to the highest PSNR.

(2) Effectiveness of improvements

The outperformance of the proposed method can be attributed to the pose classification module and ℓ_0 loss function. The pose classification module distinguishes the yarn poses to classify varying degrees of defocus blur, because different poses correspond to different out-of-focus distances. In this way, images with different defocus degrees can be fed into different deblurring channels for differentiated deblurring, instead of arbitrarily indifference processing for all images. The ℓ_0 loss function minimises the gradient loss between pixels to guide the model to focus on the deblurring of the edge details of the yarn body, because the edge of the yarn at the junction with the background changes strongly in pixel gradient. Under the combined effect, the proposed model outperforms other models.

To further evaluate the performance gains from the pose classification module and the ℓ_0 loss function, the proposed method is further compared with the network removing pose classification module, and ℓ_0 loss function. The quantitative results and visual comparisons are respectively reported in Figure 9.

As shown in Figure 9(a), removing the pose classification module reduces 3.3149% of the average PSNR value, while removing the ℓ_0 loss function has basically no effect on PSNR. It is observed that the proposed pose classification module is beneficial for variable-scale deblurring of yarn images in spinning. As shown in Figure 9(b), removing the pose classification module (only keep ℓ_0 regularisation in loss function) causes the gradient curve to steepen sharply near the value of 0, while using the normal loss function without ℓ_0 regularisation causes the nonzero gradient values to be denser. It is observed that the ℓ_0 regularisation is beneficial for the restoration of image edges. However, only keeping the ℓ_0 loss function for all kinds of blurry yarn images without the pose classification module will result in an excessive sharpening edge of the yarn body and distortion of the entire image. The visual results in Figure 9(c) also illustrate that integrating the pose classification module and the improved loss function achieves a

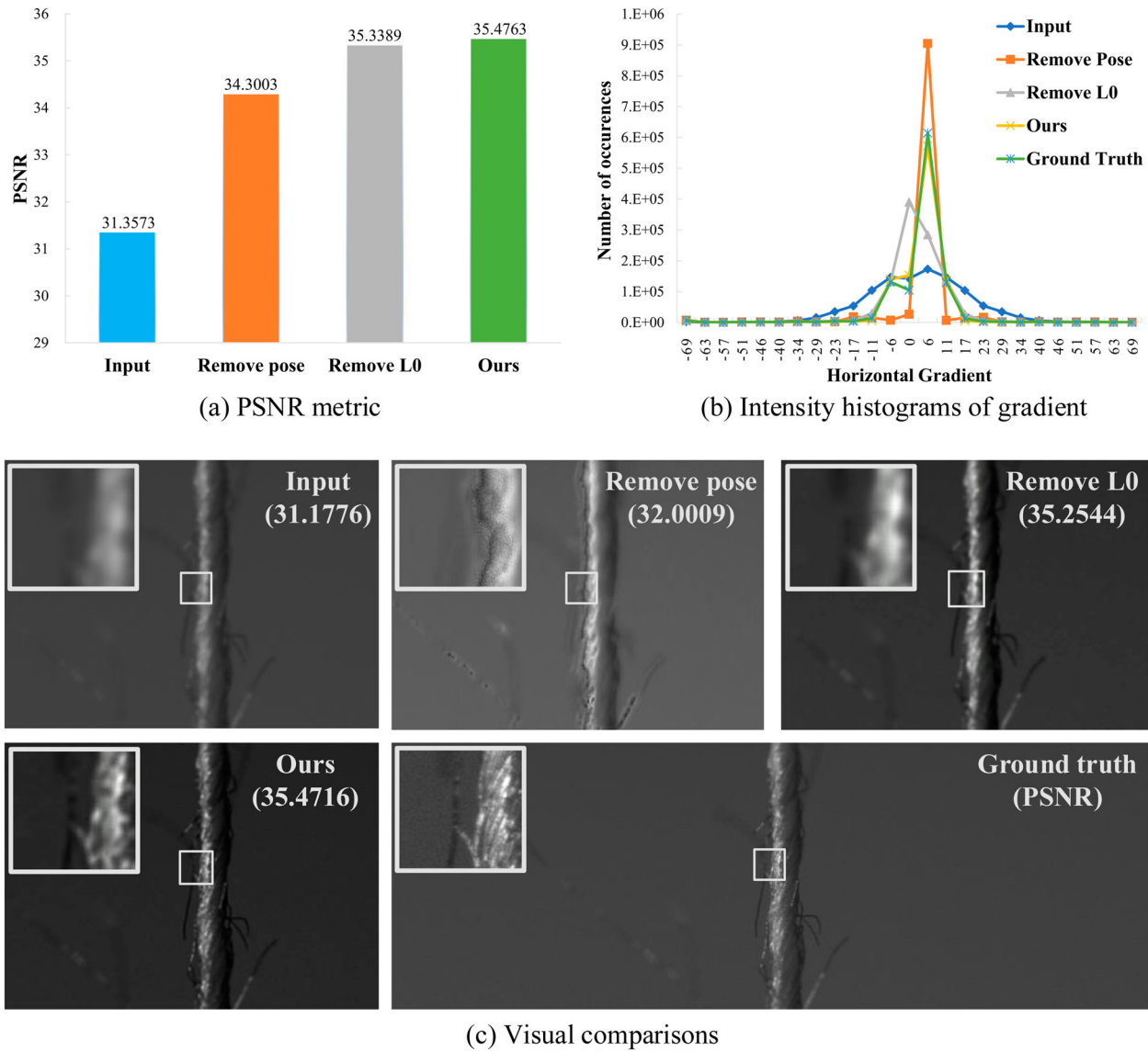


Figure 9. Comparisons of the proposed KD-DeblurNet, removing pose, and removing ℓ_0 .

better deblurring effect of the yarn image closer to the ground truth.

5. Conclusion and future work

This paper proposed a new approach via knowledge augmented deep learning modelling to deblur yarn images in dynamic spinning scenes with variable-scale defocusing. It was beneficial to timely and accurate detection of product quality abnormalities, thereby improving product quality and reducing production losses. By investigating the movement of the yarn in spinning, the prior knowledge between yarn poses and defocus blur degrees was excavated to guide the construction of the deblurring neural network. Benefit from the prior knowledge embedded improvement for deep learning model, the proposed method outperformed

state-of-the-art methods for yarn image deblurring, which provided more accurate input for yarn quality detection.

Future work will focus on abstracting a general deblurring model for more scenarios characterised by variable-scale and edge details, which can adaptively learn the knowledge of different industrial fields.

Notes on contributors



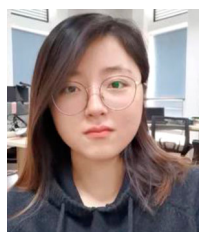
Chuqiao Xu received the M.S. degree in mechanical engineering from Xinjiang University, Urumchi, China, in 2017. He is currently working toward the Ph.D. degree in big data driven product quality inspection for industrial engineering at School of Mechanical Engineering, Shanghai Jiao Tong University, Shanghai, China.

His current research focuses on big data analytics and computer vision solutions for yarn spinning systems.



Junliang Wang received the B.S. degree in scheduling of manufacturing systems from Wuhan University of Technology, Wuhan, China, in 2009 and the Ph.D. degree in big data driven operation for industrial engineering at School of Mechanical Engineering, Shanghai Jiao Tong University, Shanghai, China, in 2018.

Since 2018, he is a Research Assistant with College of Mechanical Engineering, Donghua University, Shanghai, China. He is the author of 2 books, more than 30 articles. His current research focuses on big data analytics and operation in complex manufacturing systems.



Jing Tao received the Bachelor's degree in mechanical engineering from Donghua University, Shanghai, China, in 2020. She is currently working towards the M.S. degree in mechanical engineering at Donghua University. Her current research focuses on computer vision.



Jie Zhang received the Ph.D. degree in scheduling of manufacturing systems from Nanjing University of Aeronautics and Astronautics, Nanjing, China, in 1997. She is currently the Dean of College of Mechanical Engineering, Donghua University, Shanghai, China. Before joining Donghua University, she was a Professor

with the Institute of Intelligent Manufacturing and Information Engineering, Shanghai Jiao Tong University, Shanghai, China. She is the author of 6 books, more than 100 articles. Her research interests include industrial big data analysis, intelligent production scheduling, production control in intelligent manufacturing system, and intelligent quality analysis.



Ray Y. Zhong received the B.S. degree in mathematics and computer science and technology from Gannan Normal University, Ganzhou, China, in 2004, the M.S. degree in signal and information processing from the Guangdong University of Technology, Guangzhou, China, in 2009, and the Ph.D. degree in industrial and

manufacturing systems engineering from the University of Hong Kong, Hong Kong, in 2013. He is now an Assistant Professor with the Department of Industrial and Manufacturing Systems Engineering, University of Hong Kong. His current research interests include big data in manufacturing and service, advanced planning and scheduling, and RFID in Internet of manufacturing things. Dr. Zhong is a member of CIRP RA, Logistics and Supply Chain Management Hong Kong, Institution of Engineering and Technology, American Society of Mechanical Engineers, and IEEE. Ray was awarded the 2018 IJPR Best Paper with the title of 'Big Data Analytics for Physical Internet-based intelligent manufacturing shop floor,' Best Conference Paper Award with the title of 'Analysis of RFID Datasets for Smart Manufacturing Shop Floors' in 15th IEEE International Conference on Networking, Sensing

and Control, New Zealand Chinese Youth Scientist Award (NZCYSA) 2017 and the Young Author Prize in the 15th IFAC/IEEE/IFIP/IFORS Symposium on Information Control Problems in Manufacturing.

Disclosure statement

No potential conflict of interest was reported by the author(s).

Funding

This work was supported by Shanghai Science and Technology Project: [Grant Number 19411951506], The Fundamental Research Funds for the Central Universities: [Grant Number 2232021A-08], Shanghai Chenguang Program: [Grant Number 20CG41].

Data availability statement

The data that support the findings of this study are available on request from the corresponding author, J. Zhang. The data are not publicly available due to their containing information that could compromise the privacy of cooperative enterprise.

ORCID

Chunqiao Xu <http://orcid.org/0000-0001-5611-2990>

Jie Zhang <http://orcid.org/0000-0002-6215-0237>

Ray Y. Zhong <http://orcid.org/0000-0002-3011-2009>

References

- Abang, M. Z., M. S. Ramli, and S. A. Halim. 2018. "Application of Blind Deconvolution and Lucy-Richardson Deconvolution for Image Deblurring." *Journal of Fundamental and Applied Sciences* 9 (5S): 232–244. doi:10.4314/jfas.v9i5s.17.
- Beck, A., and M. Teboulle. 2009. "Fast Gradient-Based Algorithms for Constrained Total Variation Image Denoising and Deblurring Problems." *IEEE Transactions on Image Processing* 18 (11): 2419–2434. doi:10.1109/TIP.2009.2028250.
- Cai, J., W. Zuo, and L. Zhang. 2020. "Dark and Bright Channel Prior Embedded Network for Dynamic Scene Deblurring." *IEEE Transactions on Image Processing* 29: 6885–6897. doi:10.1109/TIP.2020.2995048.
- Chakrabarti, A. 2016. "A Neural Approach to Blind Motion Deblurring." Paper presented at the European Conference on Computer Vision, Cham, September 17. doi:10.1007/978-3-319-46487-9_14.
- Chen, J., Z. Zhang, and F. Wu. 2020. "A Data-Driven Method for Enhancing the Image-Based Automatic Inspection of IC Wire Bonding Defects." *International Journal of Production Research* 59 (16): 4779–4793. doi:10.1080/00207543.2020.1821928.
- Cheng, S., R. Liu, Y. He, X. Fan, and Z. Luo. 2020. "Blind Image Deblurring via Hybrid Deep Priors Modeling." *Neurocomputing* 387: 334–345. doi:10.1016/j.neucom.2020.01.004.

- Fan, Q., H. Huang, Y. Li, Z. Han, Y. Hu, and D. Huang. 2021. "Beetle Antenna Strategy Based Grey Wolf Optimization." *Expert Systems with Applications* 165: 113882. doi:10.1016/j.eswa.2020.113882.
- Ferrada, H., C. A. Navarro, and N. Hirschfeld. 2020. "A Filtering Technique for Fast Convex Hull Construction in R2." *Journal of Computational and Applied Mathematics* 364: 112298. doi:10.1016/j.cam.2019.06.014.
- Gao, H., X. Tao, X. Shen, and J. Jia. 2019. "Dynamic Scene Deblurring with Parameter Selective Sharing and Nested Skip Connections." Paper presented at the 2019 IEEE/CVF Conference on Computer Vision and Pattern Recognition (CVPR), Long Beach, June 15–20. doi:10.1109/CVPR.2019.00397.
- Genta, G., M. Galetto, and F. Franceschini. 2020. "Inspection Procedures in Manufacturing Processes: Recent Studies and Research Perspectives." *International Journal of Production Research* 58 (15): 4767–4788. doi:10.1080/00207543.2020.1766713.
- Guha, A., C. Amarnath, S. Pateria, and R. Mittal. 2010. "Measurement of Yarn Hairiness by Digital Image Processing." *The Journal of The Textile Institute* 101 (3): 214–222. doi:10.1080/00405000802346412.
- Jing, J., H. Li, H. Zhang, Z. Su, and K. Zhang. 2020. "Detection of Bobbin Yarn Surface Defects by Visual Saliency Analysis." *Fibers and Polymers* 21 (11): 2685–2694. doi:10.1007/s12221-020-9728-8.
- Khan, S. U., I. U. Haq, S. Rho, S. W. Baik, and M. Y. Lee. 2019. "Cover the Violence: A Novel Deep-Learning-Based Approach Towards Violence-Detection in Movies." *Applied Sciences* 9 (22): 4963. doi:10.3390/app9224963.
- Kupyn, O., V. Budzan, M. Mykhailych, D. Mishkin, and J. Matas. 2018. "DeblurGAN: Blind Motion Deblurring Using Conditional Adversarial Networks." Paper presented at the 2018 IEEE/CVF Conference on Computer Vision and Pattern Recognition (CVPR), Salt Lake City, June 18–23. doi:10.1109/CVPR.2018.00854.
- Kusiak, A. 2020. "Convolutional and Generative Adversarial Neural Networks in Manufacturing." *International Journal of Production Research* 58 (5): 1594–1604. doi:10.1080/00207543.2019.1662133.
- Li, Z., N. Xiong, J. Wang, R. Pan, W. Gao, and N. Zhang. 2017. "An Intelligent Computer Method for Automatic Mosaic of Sequential Slub Yarn Images Based on Image Processing." *Textile Research Journal* 88 (24): 2854–2866. doi:10.1177/0040517517732081.
- Luo, T., R. Fan, Z. Chen, X. Wang, and D. Chen. 2019. "Deblurring Streak Image of Streak Tube Imaging Lidar Using Wiener Deconvolution Filter." *Optics Express* 27 (26): 37541–37551. doi:10.1364/OE.27.037541.
- Nah, S., T. H. Kim, and K. M. Lee. 2017. "Deep Multi-Scale Convolutional Neural Network for Dynamic Scene Deblurring." Paper presented at the 2017 IEEE Conference on Computer Vision and Pattern Recognition (CVPR), Honolulu, July 21–26. doi:10.1109/CVPR.2017.35.
- Perng, D., S. Lee, and C. Chou. 2010. "Automated Bonding Position Inspection on Multi-Layered Wire IC Using Machine Vision." *International Journal of Production Research* 48 (23): 6977–7001. doi:10.1080/00207540903059497.
- Rai, R., M. K. Tiwari, D. Ivanov, and A. Dolgui. 2021. "Machine Learning in Manufacturing and Industry 4.0 Applications." *International Journal of Production Research* 59 (16): 4773–4778. doi:10.1080/00207543.2021.1956675.
- Sha, L., D. Schonfeld, and J. Wang. 2020. "Graph Laplacian Regularization with Sparse Coding for Image Restoration and Representation." *IEEE Transactions on Circuits and Systems for Video Technology* 30 (7): 2000–2014. doi:10.1109/TCSVT.2019.2913411.
- Sun, J., W. Cao, Z. Xu, and J. Ponce. 2015. "Learning a Convolutional Neural Network for Non-Uniform Motion Blur Removal." Paper presented at the 2015 IEEE Conference on Computer Vision and Pattern Recognition (CVPR), Boston, June 7–12. doi:10.1109/CVPR.2015.7298677.
- Tao, X., H. Gao, X. Shen, J. Wang, and J. Jia. 2018. "Scale-Recurrent Network for Deep Image Deblurring." Paper presented at the 2018 IEEE/CVF Conference on Computer Vision and Pattern Recognition, Salt Lake City, June 18–23. doi:10.1109/CVPR.2018.00853.
- Wan, S., S. Tang, X. Xie, J. Gu, R. Huang, B. Ma, and L. Luo. 2020. "Deep Convolutional-Neural-Network-Based Channel Attention for Single Image Dynamic Scene Blind Deblurring." *IEEE Transactions on Circuits and Systems for Video Technology* 31 (8): 2994–3009. doi:10.1109/TCSVT.2020.3035664.
- Wang, C., B. C. Jiang, Y. S. Chou, and C. C. Chu. 2011. "Multivariate Analysis-Based Image Enhancement Model for Machine Vision Inspection." *International Journal of Production Research* 49 (10): 2999–3021. doi:10.1080/00207541003801242.
- Wang, K. J., Y. H. Lee, and S. Angelica. 2020. "Digital Twin Design for Real-Time Monitoring – A Case Study of Die Cutting Machine." *International Journal of Production Research* 59 (21): 6471–6485. doi:10.1080/00207543.2020.1817999.
- Wang, M. W., F. Z. Zhu, and Y. Y. Bai. 2021. "An Improved Image Blind Deblurring Based on Dark Channel Prior." *Optoelectronics Letters* 17 (1): 40–46. doi:10.1007/s11801-021-0081-y.
- Wu, J., Q. Li, S. Liang, and S. Kuang. 2020. "Convolutional Neural Network with Squeeze and Excitation Modules for Image Blind Deblurring." Paper presented at the 2020 Information Communication Technologies Conference (ICTC), Nanjing, May 29–31. doi:10.1109/ICTC49638.2020.9123259.
- Xu, Z., H. Chen, and Z. Li. 2020. "Blind Image Deblurring via the Weighted Schatten p-Norm Minimization Prior." *Circuits, Systems, and Signal Processing* 39 (12): 6191–6230. doi:10.1007/s00034-020-01457-z.
- Xu, C., J. Wang, J. Zhang, and C. Lu. 2020. "A New Welding Path Planning Method Based on Point Cloud and Deep Learning." Paper presented at the 2020 IEEE 16th International Conference on Automation Science and Engineering (CASE), Hong Kong, Aug. 20–21. doi:10.1109/CASE48305.2020.9216866.
- Yan, Y., W. Ren, Y. Guo, R. Wang, and X. Cao. 2017. "Image Deblurring via Extreme Channels Prior." Paper presented at the 2017 IEEE Conference on Computer Vision and Pattern Recognition (CVPR), Honolulu, July 21–26. doi:10.1109/CVPR.2017.738.
- Zhang, Y., Y. Shi, L. Ma, J. Wu, L. Wang, and H. Hong. 2021. "Blind Natural Image Deblurring with Edge Preservation Based on L0-Regularized Gradient Prior." *Optik* 225: 165735. doi:10.1016/j.ijleo.2020.165735.
- Zhao, H., Z. Ke, N. Chen, S. Wang, K. Li, L. Wang, X. Gong, et al. 2020. "A New Deep Learning Method for Image Deblurring in Optical Microscopic Systems." *Journal of Biophotonics* 13 (3): e201960147. doi:10.1002/jbio.201960147.

- Zhong, Z., and Z. Ma. 2021. "A Novel Defect Detection Algorithm for Flexible Integrated Circuit Package Substrates." *IEEE Transactions on Industrial Electronics*. doi:[10.1109/TIE.2021.3057026](https://doi.org/10.1109/TIE.2021.3057026).
- Zhou, K., P. Zhuang, J. Xiong, J. Zhao, and M. Du. 2020. "Blind Image Deblurring with Joint Extreme Channels and

L0-Regularized Intensity and Gradient Priors." Paper presented at the Proceedings – International Conference on Image Processing (ICIP), Abu Dhabi, September 25-28. doi:[10.1109/ICIP40778.2020.9191010](https://doi.org/10.1109/ICIP40778.2020.9191010).

Copyright of International Journal of Production Research is the property of Taylor & Francis Ltd and its content may not be copied or emailed to multiple sites or posted to a listserv without the copyright holder's express written permission. However, users may print, download, or email articles for individual use.